STUDY ON COOLING OF BIONIC LEAF-VEIN CHANNEL LIQUID-COOLED PLATE FOR LITHIUM-ION BATTERY PACK

Guangqiang SUN, Zhiqiang LI*, Fang WANG, Xianfei LIU, Yichun BA

School of Energy and Environment, Zhongyuan University of Technology, Zhengzhou, Henan 450007 China

*Corresponding author; Email: lzqwin@126.com

In order to improve the cooling effect of lithium-ion battery packs, a bionic leaf-vein channel liquid-cooled plate was proposed. The liquid-cooled plate was numerically simulated using ANSYS FLUENT. The results show that at different Reynolds numbers, the pressure drop of the bionic leaf-vein channel is always smaller than that of the serpentine channel, and the local pressure drop of the bionic leaf-vein channel is 88.43% lower than that of the serpentine channel. The pressure drop of the bionic leaf-vein channel increases gradually with the increase of the branching angle, the branching angle increases from 35° to 45°, and the pressure drop increases by 212.27 Pa. The Reynolds number increases from 500 to 7500, and the maximum temperature of the lithium-ion battery pack reduces by 3.74 K, and the maximum temperature difference reduces by 2.25 K.

Key words*: thermal management system, bionic channel, liquid cooling strategy*

1. Introduction

In recent years, the cooling requirements for heat generating devices in limited space have become higher and higher. Lithium-ion batteries (LIBs) in electric vehicles (EVs) and energy storage power stations are typical heat generating devices that require cooling in a limited space.

At present, the commonly used cooling methods mainly include air cooling, phase change material (PCM) cooling and liquid cooling. Air cooling has the advantages of low cost and high safety [1,2]. However, due to the small specific heat capacity of air, it is difficult to take away a large amount of heat in a short time [3,4]. PCM will absorb a lot of heat during phase change to achieve the purpose of reducing the temperature of the cooled equipment. PCM cooling has the advantage of lightweight and compact [5]. However, it is difficult to achieve the cooling effect by using PCM alone in a limited space [6,7]. Although liquid cooling system has the possibility of leakage, the liquid cooling system can take away a lot of heat in a short time, which is suitable for the heat dissipation of equipment in limited space [8-10].

The maximum temperature (T_{max}) and maximum temperature difference (ΔT_{max}) of the cooled equipment are important parameters to measure the cooling system. At the same time, the energy consumption of the cooling system itself is also an important standard to measure the cooling system. The liquid-cooled plate is an important part of the liquid cooling system, and its performance has a great impact on the cooling system. In order to improve the cooling capacity of the liquid cooling system and reduce the pressure drop of the liquid-cooled plate, many researchers have made many

optimizations of the existing liquid-cooled plate or designed many new liquid-cooled plates. Kuang *et al.* [11] designed a micro pin-fin heat sink that can effectively improve heat transfer capacity and inhibit temperature rise. Ren *et al.* [12] designed a liquid-cooled plate with variable microchannels to improve the temperature uniformity of the cooled object. The simulation and experimental results show that the liquid-cooled plate has better cooling performance. Koorata *et al.* [13] proposed a battery thermal management system (BTMS) based on microchannel liquid-cooled plates, which can improve the temperature uniformity of soft pack batteries by more than 140%. Wang *et al.* [14] proposed a plate fin-and-tube heat exchanger with ring-bridge slit fins, and obtained the optimal fin structure by orthogonal experiment. Joshi *et al.* [15] computationally analyzed a passive heating system using fins and PCMs and investigated the effect of different PCM thicknesses on heat transfer at low temperatures. Talele *et al.* [16] used a numerical model of thermal runaway to explain the evolution of the thermal runaway trigger point under different cathode chemical conditions under the influence of ambient temperature changes. Yang *et al.* [17] found that the cell temperature rise of solid-state batteries is mainly affected by reversible heat, and the heat of polarization is the largest contributor to the total heat generation of solid-state batteries. Chen *et al.* [18] developed a battery state-of-health estimation model based on convolutional neural networks, which can estimate the state-of- health of a battery from constant-current charge and discharge data. Subhedar *et al.* [19] conducted a study for immersion cooling system and found that Al_2O_3/EG-water nano coolant with a volume fraction of 4% or higher can maintain the battery temperature up to 50℃.

A bionic leaf-vein channel liquid-cooled plate was designed to cope with the high T_{max} and large ΔT_{max} of LIB packs during high-rate discharge. The microscopic flow in the channel of the bionic leaf-vein channel and the serpentine channel is analyzed to compare the pressure drop characteristics and cooling performance of the two liquid-cooled plates. The relationship between the branch angle of the bionic leaf-vein channel and the pressure drop was determined. The cooling performance of the bionic leaf-vein channel liquid-cooled plate is investigated under different Reynolds numbers (Re) and different charge and discharge rates of LIB. To provide a reference for the future application of bionic channels or the application of bionic leaf-vein channel liquid-cooled plates in hybrid BTMS.

2. Numerical Methods

2.1 The bionic leaf-vein channel liquid-cooled plate

Fig. 1 is the schematic diagram of the bionic leaf-vein channel liquid-cooled plate. The bionic leaf-vein channel liquid-cooled plate is made of aluminum. The size of the bionic leaf-vein channel liquid-cooled plate is 168×216 mm, and the thickness is 4 mm. The size of the bionic leaf-vein channel liquid-cooled plate can be scaled according to the heat output and size of the cooled object. The channel in the liquid-cooled plate was designed with the leaf-vein channel as the prototype. The inlet and outlet of the channel are

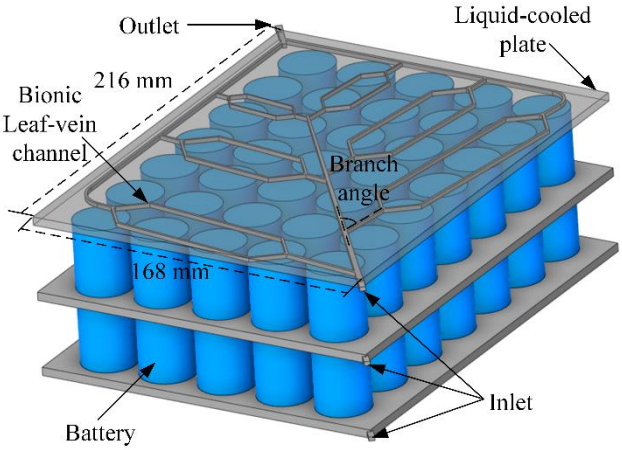

Fig. 1 Bionic leaf-vein channel liquid-cooled plate system diagram

rectangular, and the width of the channel changes gradually. The coolant flowing in the bionic leaf-vein channel uses an aqueous 50% concentration of ethylene glycol, which is more widely used today, and its thermophysical properties are shown in Table 1.

Table 1. Thermophysical properties of coolant

Medium	ρ [kg/m^3]	C_p [Jkg^{-1}K^{-1}]	k [Wm^{-1}K^{-1}]	Dynamic viscosity [P$_a$s]
coolant	1071	3300	0.384	0.00103

2.2 Mathematical Methods

In the numerical calculation, the following assumptions are made to simplify the calculation: (1) The thermal resistance and thermal conductivity of the aluminum material in the bionic leaf-vein channel liquid-cooled plate are uniform. (2) The physical properties of materials in numerical simulation are independent of temperature [20]. Based on the above assumptions, the transient heat transfer equation of the bionic leaf-vein channel liquid-cooled plate can be written as follows:

$$\rho C_P \frac{\partial T}{\partial t} = k_x \frac{\partial^2 T}{\partial x^2} + k_y \frac{\partial^2 T}{\partial y^2} + k_z \frac{\partial^2 T}{\partial y^2} + Q \tag{1}$$

where ρ_b, C_{pb} and T_b indicate the density, specific heat capacity and temperature of the battery respectively. Q is the heat generated by the lithium battery, and t is the time and k_x, k_y, k_z are the heat transfer coefficients of the battery in the three directions x, y, z respectively.

The flow process of coolant in the bionic leaf-vein channel is calculated according to the forced flow of incompressible fluid, and the physical process of flow heat transfer is represented by continuity equation, momentum conservation equation and energy conservation equation [21,22].

Continuity equations for incompressible fluids:

$$\nabla \cdot (\rho_c \overrightarrow{v_c}) = 0 \tag{2}$$

Momentum conservation equation:

$$\frac{\partial}{\partial t}(\rho_c \overrightarrow{v_c}) + \nabla \cdot (\rho \overrightarrow{v_c} \overrightarrow{v_c}) = -\nabla P + \nabla \cdot (\mu_c \nabla \overrightarrow{v_c}) \tag{3}$$

Energy conservation equation:

$$\frac{\partial (\rho_c C_{pc} T_c)}{\partial t} + \nabla \cdot (\rho_c C_{pc} T_c \overrightarrow{v_c}) = \nabla \cdot (k_c \nabla T_c) \tag{4}$$

The Re is defined as:

$$Re = \frac{\rho_c D v_c}{\mu_c} \tag{5}$$

where ρ_c, C_{pc}, v_c, μ_c, T_c, k_c, P and D represent the density, specific heat capacity, velocity vector, dynamic viscosity, temperature, thermal conductivity, pressure of the fluid respectively, and equivalent diameter.

The bionic leaf-vein channel in this study is a rectangular runner and its equivalent diameter should be obtained before performing the Re calculation. The equivalent diameter of the rectangle can be calculated according to Eq. 6.

$$D = \frac{2ab}{a+b} \tag{6}$$

Where a and b represent the width of the rectangle and the height of the rectangle respectively.

In this study the height of the inlet of the bionic leaf-vein channel is 2 mm and the width is 2.67 mm, and D=2×2×2.67/(2+2.67)=2.287 mm. when the inlet flow rate of coolant is 0.21 m/s Re=0.21 ×2.287×10^{-3}×1071/0.00103=500. Using the same calculation method, Re=2500 when the coolant inlet flow rate is 1.05 m/s. Re=5000 when the coolant inlet flow rate is 2.10 m/s. Re=7500 when the coolant inlet flow rate is 3.15 m/s.

2.3 Numerical Calculation

ANSYS FLUENT was used for numerical solution. The boundary condition of the inlet of the bionic leaf-vein channel is velocity inlet and the boundary condition of the outlet is pressure outlet. The inlet temperature of the coolant and the ambient temperature are both 298.15 K. The temperature of the return air at the outlet of the bionic leaf-vein channel is the ambient temperature. The interface between the LIB pack and air contact is set as natural convection heat transfer, and the natural convection heat transfer coefficient is 5 $Wm^{-3}K^{-1}$. The coupling method of pressure and velocity is Coupled. The pressure and velocity are coupled by the coupling method, and the discrete formats for pressure, momentum, energy and time are all second-order upwind formats. The surface of the coolant channel is set with a non-slip wall. The time step in the calculation is 1s, and the number of steps is determined according to the time of one charge and discharge cycle at different charge and discharge multiples of 26650 LIBs. (One charging cycle of 26650 LIB at 1C charging and discharging multiplicity is 4320 s.)

3D Modeling with ANSYS SpaceClaim. The mesh was performed using Fluent Meshing. The mesh types in the computational domain are all Polyhedral. the minimum Orthogonal Quality of the mesh is 0.38. In the working conditions of Section 3.1 and 3.4, the Re of the coolant in the bionic leaf-vein channel is greater than 2000 and the flow is turbulent. The standard K-Epsilon model was used for turbulence modeling in the numerical simulation of turbulent flow conditions [12]. The value of y+ near the wall is 81 for Re 7500. y+ near the wall is 53 for Re 5000. y+ near the wall is 31 for Re 2500.

In order to ensure the accuracy and efficiency of the calculation, the number of grids is verified independently. Under the condition of Re of 500 and heat flux of the bionic leaf-vein channel liquid-cooled plate of 500 W/m^2, the number of grids of 96543, 107989, 118599, 127567 and 139053 were used to calculate, respectively. The T_{max} and minimum temperature (T_{min}) of the bionic leaf-vein channel liquid-cooled plate in the calculation are shown in Fig. 2. It can be seen from Fig. 2 that after the number of grids reaches 118,599, the T_{max} and T_{min} of the bionic leaf-vein channel liquid-cooled plate hardly change after the number of grids continues to increase, so the number of 118,599 grids is used for calculation.

2.4 Experimental verification

In order to ensure the accuracy of the numerical simulation, the experimental method is used to verify the numerical simulation. The

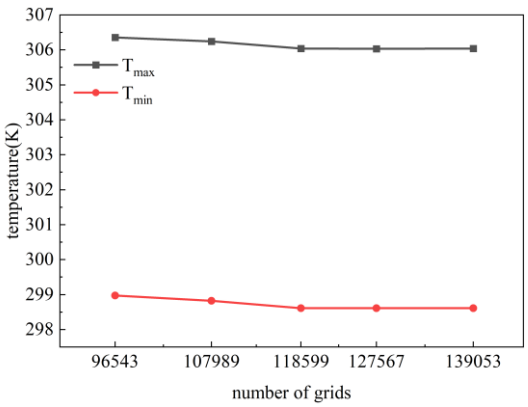

Fig. 2 Grid independence verification

schematic diagram of the experiment is shown in Fig. 3, and the physical diagram is shown in Fig. 4. The PI heating film with internal resistance of 8Ω (produced by Shenzhen Sanying New Material Technology Co., LTD.) is used to generate heat according to the calorific value of 26650 LIB pack to replace the heat of the LIB pack. High-power programmable DC power supply (produced by Hangzhou Lanyi Electronics Co., LTD.) supplies power to PI heating film. The K-type thermocouple measures the temperature in the middle of the liquid-cooled plate. And the data acquisition instrument transmits the collected temperature data to the computer. The cistern is filled with coolant and a submersible pump is placed as a power device.

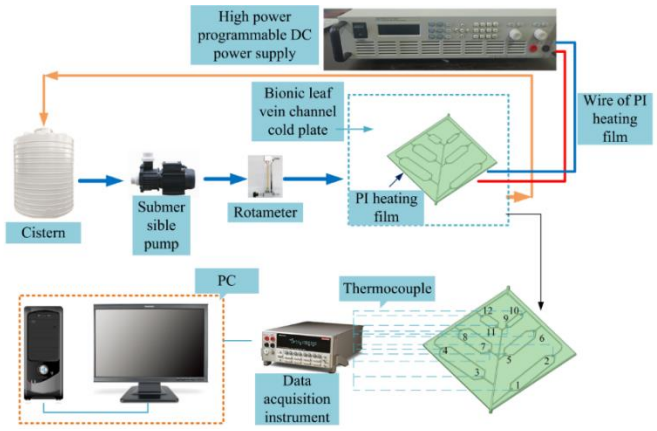

Fig. 3 Experimental schematic diagram

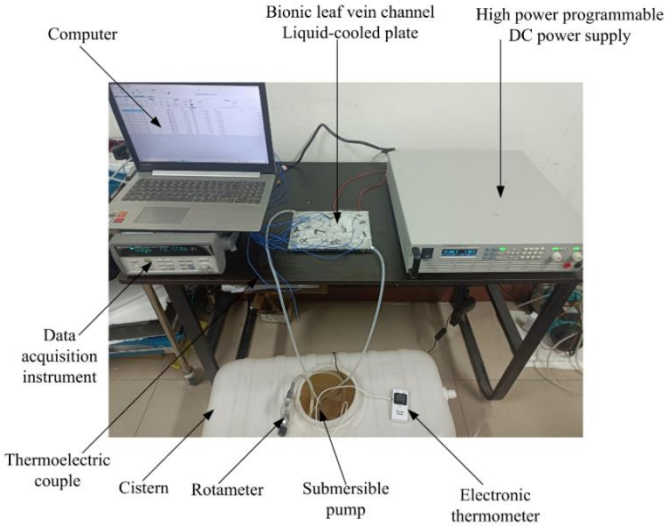

Fig. 4 Physical diagram of experimental device

The liquid-cooled plate is formed by pasting and fixing two parts after processing respectively. The liquid-cooled plate is formed by pasting and fixing two parts after processing respectively. The upper part of the liquid-cooled plate is made of acrylic material. And the bionic leaf-vein channel is engraved on it by Computer Numerical Control (CNC) engraving. The lower part of the liquid-cooled plate is an aluminum plate of the same shape and size as the upper part but without the channel. One side of the aluminum plate is bonded with the acrylic plate, the other side is affixed with the PI heating film. The position where the PI heating film meets the air is affixed with thermal insulation material. A total of 12 temperature measuring points are arranged on the liquid-cooled plate. On the acrylic plate, the corresponding position of the measuring point has a round hole, and the temperature

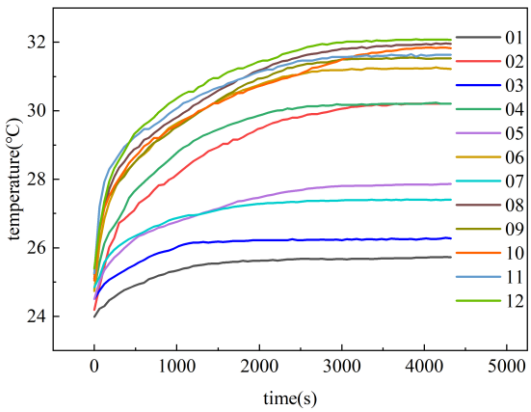

(a) Temperature change at the point of measurement

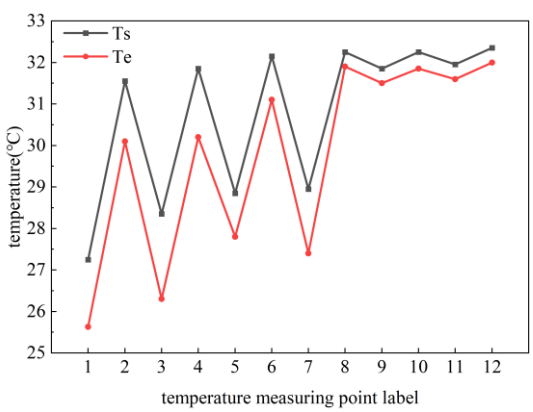

5 (b) Comparison between experimental and simulated data

Fig. 5 Temperature change and comparison between experimental and simulated

probe of the thermocouple is placed in the round hole to measure the temperature at the interface of the acrylic plate and the aluminum plate, that is, the central section of the liquid-cooled plate.

The temperature variations at 12 measurement points during the experiment measured using the K-type thermocouple and the Keysight model 34972A data acquisition instrument (with a measurement error of 0.1%) are shown in Fig. 5(a). The temperatures at the end of discharge at 12 measurement points in the middle plane of the liquid-cooled plate obtained by numerical simulation and experiment were compared under the working condition of 500 W/m^2 of heat production, and the results are shown in Fig. 5(b). The trend of the temperature obtained from experiment and numerical simulation is consistent, and the maximum difference is 2.05℃, with an error of 7.23%. After experimental verification, the accuracy of numerical simulation can be guaranteed.

3. Results and discussion

3.1 Pressure drops characteristics of liquid-cold plate at different Re

According to the balance between the heat generated by the LIB and the heat taken away by the coolant, Re is set at 500. In order to investigate the quantitative relationship between Re and pressure drop, the Re was enlarged by 5, 10 and 15 times, respectively. Fig. 6 compares the pressure drop of bionic leaf-vein channel liquid-cooled plate and serpentine channel liquid-cooled plate with almost the same channel heat transfer area at different Re (bionic leaf-vein channel liquid-cooled plate: 10835 mm^2, serpentine channel liquid-cooled plate: 9990 mm^2). When Re is 500, the pressure drop of serpentine channel liquid-cooled plate is 2.19 kPa, that of bionic leaf-vein channel liquid-cooled plate is 0.99 kPa, and the pressure drop of bionic leaf-vein channel liquid-cooled plate is 45.21% of that of serpentine channel liquid-cooled plate. When Re is 7500, the pressure drop of serpentine channel liquid-cooled plate is 101.74 kPa, that of bionic leaf-vein channel liquid-cooled plate is 58.39 kPa, and the pressure drop of bionic leaf-vein channel liquid-cooled plate is 57.39% of that of serpentine channel liquid-cooled plate. In the process of increasing Re, the pressure drops of the bionic leaf-vein liquid-cooled plate is always smaller than that of the serpentine channel liquid-cooled plate. The Re increases by 15 times from 500 to 7500, while the pressure drop of the serpentine channel liquid-cooled plate increases by 46.46 times and that with bionic leaf-vein channel liquid-cooled plate increases by 58.98 times. The increasing factor of pressure drop of bionic leaf-vein channel liquid-cooled plate and serpentine channel liquid-cooled plate is much larger than that of Re. Under the premise of meeting the cooling requirements, the value of the smaller Re should be preferred.

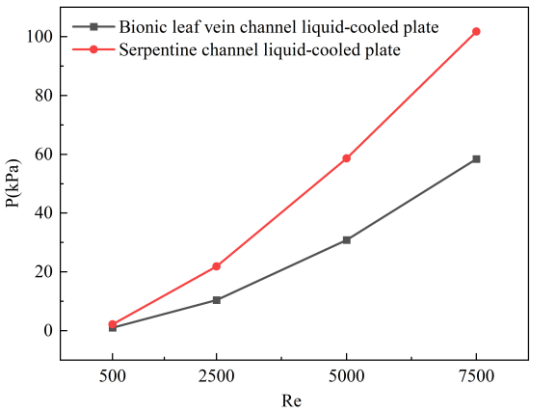

Fig. 6 Pressure drop at different Reynolds numbers

This section explores the reason why the pressure drop of the bionic leaf-vein channel liquid-cooled plate is smaller than that of the serpentine channel liquid-cooled plate. The flow resistance is composed of running resistance and local resistance. The proportion of local resistance in the total resistance is much higher than that of running resistance. The pressure drop of liquid-cooled plate is mainly affected by local resistance. The local resistance of the serpentine channel is mainly generated at the bend of the channel. Fig.7 (a) shows the flow velocity cloud diagram in the serpentine channel liquid-cooled plate when the Re is 5000. Due to the effect of centrifugal force, except for the boundary layer, the velocity away from the center of the curve is larger, and the velocity near the center of the curve is smaller. Fig.7 (b) shows the flow velocity cloud diagram in the bionic leaf-vein channel when Re is 5000 and branch angle is 45°. The local resistance of the bionic leaf-vein channel mainly appears in the branches of the channel. At the branch angle of the incoming flow direction, the velocity of the coolant is small. A relatively long-distance region with low velocity is formed near the wall of the branch angle of the incoming flow direction. The width of this region increases first and then decreases. An area of higher flow velocity is formed for a short distance at the branching angle in the direction of outflow. When the Re is 5000, the pressure drops of the coolant flowing through the first U-shaped bend in the serpentine channel is 2.42 kPa, and the pressure drop flowing through the first branch angle of the bionic leaf-vein channel is 2.14 kPa. The local pressure drop of the bionic leaf-vein channel is 88.43% of the local pressure drop of the serpentine channel. It is precisely because of the different flow state of the coolant at the local resistance of the channel that the different pressure drop characteristics of the two liquid-cooled plates are formed.

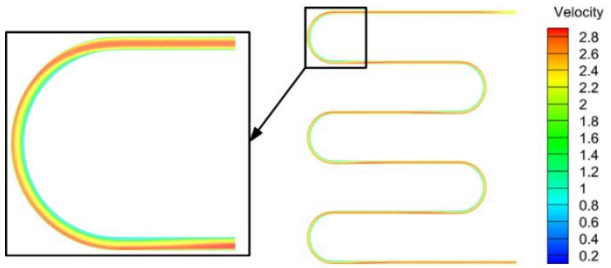

(a) Coolant flow cloud image in the serpentine channel

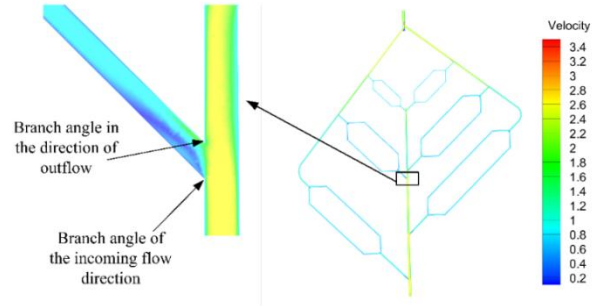

(b) Coolant flow cloud image in bionic leaf-vein channel

Fig. 7 Flow cloud image of coolant

3.2 Pressure drops characteristics at different channel branch angles

It can be seen from Fig.8 that the pressure drop of the bionic leaf-vein channel liquid-cooled plate gradually increases with the increase of the branch angle of the bionic leaf-vein channel. When the branch angle of the bionic leaf-vein channel liquid-cooled plate increases from 42.5° to 45°, the increase of pressure drop of the bionic leaf-vein channel liquid-cooled plate is much larger than the

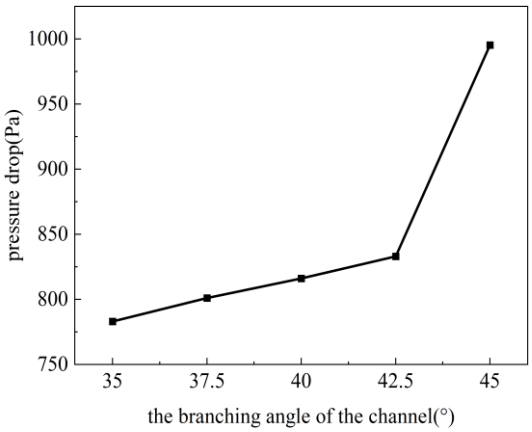

Fig. 8 Pressure drop at different branch angles

increase of other branch angles.

The phenomenon in Fig.8 was explored by intercepting the channel at the first branch angle of the bionic leaf-vein channel near the inlet of the channel to form a tee pipe of the same diameter and length as the tube in the bionic leaf-vein channel. The pressure drop of tees with different branch angles was investigated by Computational Fluid Dynamics, and the results are shown in Fig.9. As the branch angle increases, the resistance of the tee pipe also increases and the trend is the same as that of the resistance of the bionic leaf-vein channel with the branch angle. When the inlet flow rate of the coolant is the same, it can be considered that the running resistance of the tee pipe with different branch angles is the same, and the change trend of the pressure drop of the tee pipe can reflect the change of the local resistance of the tee pipe.

To sum up, with the increase of the branch angle, the local resistance at the branch of the channel increases. However, the proportion of local resistance in the flow resistance is much higher than that of running resistance. Therefore, it is shown that the pressure drops of the bionic leaf-vein channel liquid-cooled plate changes with the change of local resistance, and the local resistance increases with the increase of the branch angle of the bionic leaf-vein channel. Therefore, the pressure drops of the bionic leaf-vein channel liquid-cooled gradually increases with the increase of the branch angle of the bionic leaf-vein channel.

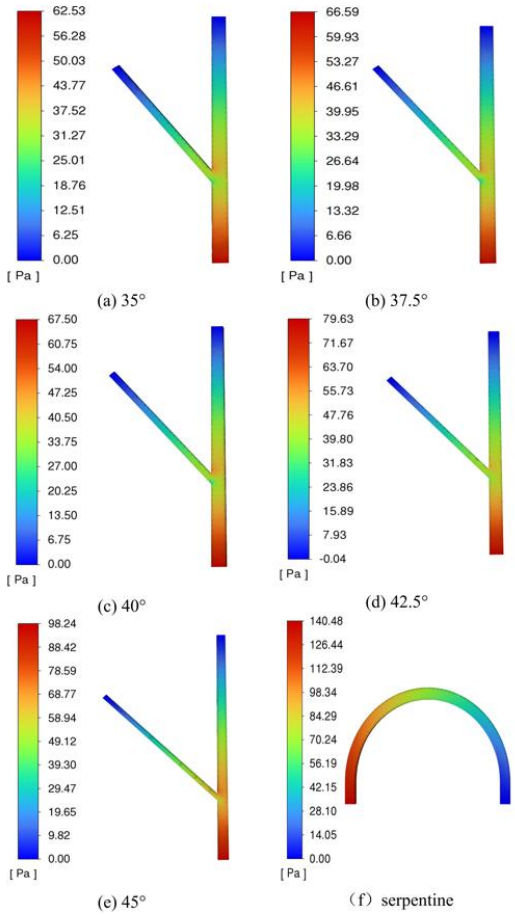

Fig. 9 Pressure drop diagram for the tee

3.3 Temperature characteristics of lithium-ion battery pack at different discharge rates

This section explores the temperature characteristics of LIB packs with different discharge rate (1C, 2C, 3C, 4C) under the cooling of bionic leaf-vein channel liquid-cooled plate. C is used to indicate the charging and discharging multiplication of a LIB and is a measurement of the charging and discharging current relative to its rated capacity. This group first charges the LIB pack by constant current charging in the preliminary experiments, and when the charging cut-off voltage of the LIB pack is reached, constant voltage charging is performed on the LIB pack to eliminate the polarization voltage. After the preliminary experimental measurements obtained 26650 LIB in 1C, 2C, 3C and 4C charging and discharging multiplicity of the average heat power of 0.5 W, 0.8 W, 1.3 W and 2.1 W, respectively [23]. In the use of FLUENT numerical simulation process will be measured experimentally in the process of LIB heat generation data loaded into the LIB pack of the solid domain. The 26650 LIB used in this paper is a lithium iron phosphate ($LiFePO_4$) battery, the positive material of the battery is $LiFePO_4$, and the negative material is carbon. The nominal voltage of the LIB is 3.2 V, the maximum charge voltage is 3.65 V, and the internal resistance of the LIB measured at AC1kHz of

50% SOC (State of Charge) is 20 mΩ. The electrolyte of lithium LIB is mainly composed of lithium hexafluorophosphate (LiPF6), solvents and additives. The physical property parameters of 26650 LIB are shown in Table 2.

Table 2. The 26650 lithium battery physical properties

Medium	ρ [kg/m^3]	C_p [Jkg^{-1}K^{-1}]	k [Wm^{-1}k^{-1}]	Diameter [mm]	Height [mm]
Battery	2218	1033	1.01/3.91	26	65

BTMS should ensure that the temperature of the LIB during the charging and discharging process is controlled at 295.15-318.15 K. Excessive temperature difference between different cells in the LIB pack may lead to thermal imbalance [24,25]. BTMS must also ensure that the ΔT_{max} between different cells in the LIB pack is less than 5 K, which is crucial for the performance and safety of the LIB pack [26,27].

When the ambient temperature is 298.15 K and Re is 2500, the highest temperature of the LIB pack at different charge and discharge rates is shown in Fig. 10 (a). With the increase of charging and discharging rate, the T_{max} of 26650 LIB pack gradually increases, but the T_{max} always meets the requirements of the highest temperature during the charging and discharging process of the LIB pack. The T_{max} of LIB pack increased from 300.11 K to 306.37 K when the charge and discharge rate increased from 1C to 4C under bionic leaf-vein channel liquid-cooled plate cooling, with an increase of 18.84%. It can be seen from Fig.10 (b) that during this process, the ΔT_{max} of the LIB pack increases from 1.68 K to 7.06 K, an increase of 76.2%. When using bionic leaf-vein channel liquid-cooled plate for LIB pack cooling, increasing the charging and discharging rate of the LIB pack results in a much larger multiplier increase in the ΔT_{max} of the LIB pack than in the T_{max}. The ΔT_{max} of the LIB pack is more than 5 K at 4C charging and discharging rate.

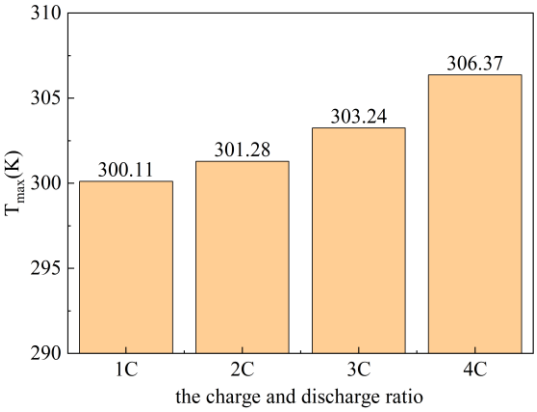

(a) Maximum temperature graph

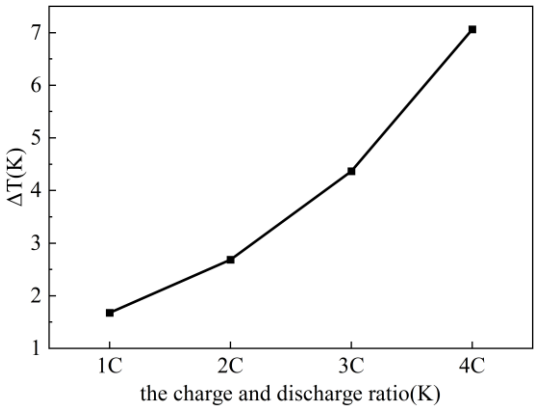

(b) The maximum temperature differences

Fig. 10 Temperature of battery pack at different charge and discharge ratios

3.4 Temperature characteristics of lithium-ion battery pack at different Re

The Re affects the temperature of the cooled LIB pack by affecting the flow pattern of the coolant in the channel of the liquid-cooled plate. The relationship between the Re and the temperature of the LIB pack was investigated at the ambient temperature of 298.15 K and the 26650 LIB 2C discharge multiplier.

From Fig.11 (a) and (b), it can be seen that with the increase of Re, the T_{max} and T_{min} of the LIB pack are gradually reduced, but the magnitudes are all decreasing. And the T_{max} of the LIB pack when the Re is 500 is in line with the T_{max} requirements of the LIB pack at work. The T_{max} of the LIB pack is almost the same in the first 250 s of the charging and discharging process under different Re. The T_{min} decreases with the increase of Re from the beginning of the charging and discharging process.

From Fig.11(c), it can be seen that with the increase of Re the ΔT_{max} of the LIB pack will gradually decrease. The decrease in the amplitude of the same will gradually decrease. When the Re is 500, it still meets the ΔT_{max} requirement of LIB pack. In the first 500 s of the charging and discharging process, the larger the Re, the larger the ΔT_{max} of the LIB pack. The main reason for this phenomenon is that the T_{max} of the LIB pack corresponding to different Re in the early charge and discharge process is almost the same, while the T_{min} gradually decreases with the increase of Re, which leads to the difference between the T_{max} and the T_{min} of the LIB pack in the early charge and discharge process with the increase of the Re. This leads to the battery charging and discharging process in the early stage of the highest temperature and the lowest temperature difference with the increase in Re, that is, the ΔT_{max} between the LIB pack with the increase in Re and increase. With the increase of the Re, the pressure drop of the liquid-cooled plate will increase rapidly, in the smaller Re can meet the cooling requirements of the cooled object should be prioritized to choose the smaller Re.

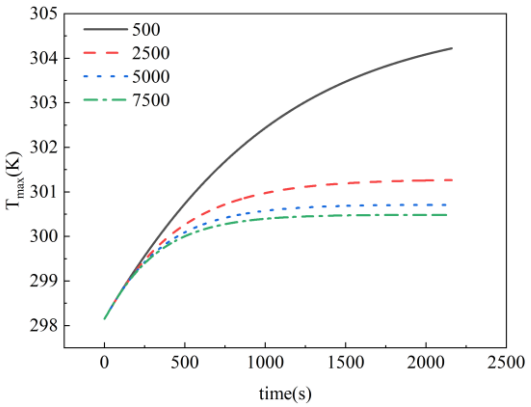

(a) Maximum temperature

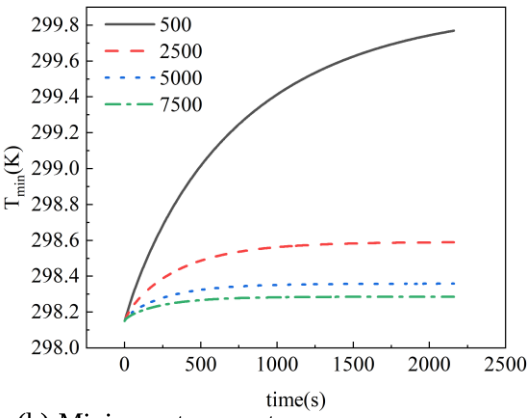

(b) Minimum temperature

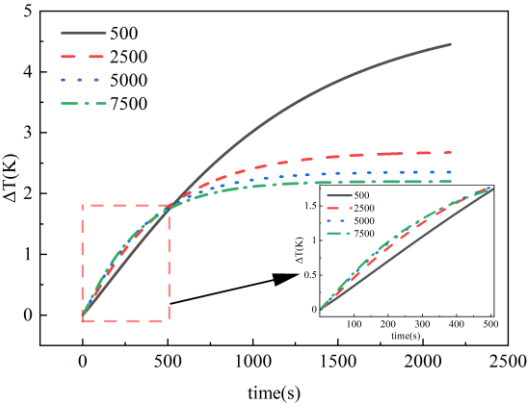

(c) Maximum temperature difference

Fig. 11 Temperature of lithium-ion battery pack at different Reynolds

3.5 Comparison of performance with serpentine channel liquid-cooled plate

This section compares the cooling capacity of the bionic leaf-vein channel liquid-cooled plate and the serpentine channel liquid-cooled plate. The T_{max} and T_{min} of 26650 LIB pack cooled by the bionic leaf-vein channel liquid-cooled plate and serpentine channel liquid-cooled plate are shown in Fig. 12(a) at both coolant and ambient temperatures of 298.15 K and a Re of 2500. The T_{max} of the LIB pack cooled by the bionic leaf-vein channel liquid-cooled plate gradually decreases with the increase of the branch angle. The T_{max} of the LIB pack cooled by the serpentine channel liquid-cooled plate is higher than the T_{max} of the LIB pack cooled by the bionic leaf-vein channel liquid-cooled plate for all branch angles. From Fig.12(b), the ΔT_{max} of the LIB pack cooled by the bionic leaf-vein channel liquid-cooled plate is

lower than that of the LIB pack cooled by the serpentine channel liquid-cooled plate when the branching angles of the bionic leaf-vein channel liquid-cooled plate are 40°, 42.5°, and 45°.

The T_{max} of the LIB packs cooled by the bionic leaf-vein channel liquid-cooled plate are lower than those of the LIB packs cooled by the serpentine channel liquid-cooled plate. Compared with the serpentine channel liquid-cooled plate, the bionic leaf-vein channel liquid-cooled plate can reduce the T_{max} and the ΔT_{max} of the LIB packs. And from section 3.1, the pressure drop of the bionic leaf-vein channel liquid-cooled plate is less than that of the serpentine channel liquid-cooled plate. The cooling performance and pressure drop characteristics of the bionic leaf-vein channel liquid-cooled plate are better than those of the serpentine channel liquid-cooled plate.

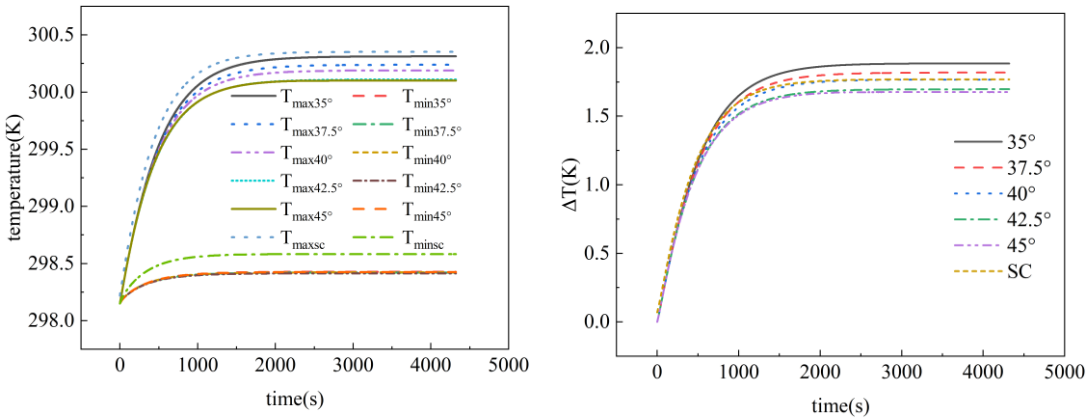

(a) Maximum temperature and minimum temperature (b) Maximum temperature difference

Fig. 12 Comparison of cooling capacity with serpentine channel liquid-cooled

4. Conclusions

With experimental validation, the following conclusions are drawn from numerical calculation studies.

(1) When the branch angle of the bionic leaf-vein channel increases from 35° to 45°, the pressure drop of the bionic leaf-vein channel increases gradually with the increase of the branch angle of the channel. When the branching angle of the bionic leaf-vein channel is increased from 42.5° to 45°, the increase in the pressure drop of the bionic leaf-vein channel is much larger than the increase in the other branching angles.

(2) At an ambient temperature of 298.15 K and a LIB charging and discharging multiplication rate of 2C, the bionic leaf-vein channel liquid-cooled plate is able to meet the temperature requirements of the LIB pack when Re is 500. With the increase of Re, the T_{max} and the ΔT_{max} of the LIB pack gradually decrease.

(3) The cooling performance and pressure drop characteristics of the bionic leaf-vein channel liquid-cooled plate are better than those of the serpentine channel liquid-cooled plate.

Acknowledgements

This work was supported by the Key Research Projects of Higher Education Institutions in Henan Province (21A470009), the Program for Science and Technology Innovation Talents in the Universities of Henan Province (20HASTIT019) and Graduate Research Innovation Program of

Zhongyuan University of Technology (YKY2023ZK12).

Nomenclature

C_p	The heat capacity [$Jkg^{-1}K^{-1}$]	Δ	Difference
D	Equivalent diameter [mm]	ρ	Density [kgm^{-3}]
k	The heat transfer coefficient [$Wm^{-1}K^{-1}$]	***Subscripts***	
Q	The heat production rate [Wm^{-3}]	b	Battery
Re	Reynolds number [$\rho_c D_e v_c/\mu_c$], [-]	c	Coolant
T	The local temperature [K]	e	Experiment
t	Time [s]	s	Simulation
T_{max}	The maximum temperature [K]	***Acronyms***	
T_{min}	The minimum temperature [K]	BTMS	Battery thermal management
ΔT_{max}	Maximum difference in temperature [K]	CNC	Computer Numerical Control
u_c	The flow rate of coolant	EV	Electric vehicle
v	The flow velocity of coolant [ms^{-1}]	LIB	Lithium-ion battery pack
Greek letters		PCM	Phase change material

References

[1] Zhang, X., *et al*., Experimental investigation on thermal management performance of electric vehicle power battery using composite phase change material, *Journal of Cleaner Production, 201* (2018), pp. 916-924

[2] Murali, G., *et al*., A review on hybrid thermal management of battery packs and it's cooling performance by enhanced PCM, *Renewable and Sustainable Energy Reviews, 150* (2021), pp. 111513

[3] Yang, C., *et al*., Structure optimization of air-cooling battery thermal management system based on lithium-ion battery, *Journal of Energy Storage, 59* (2023), pp. 106538

[4] Sharma, *et al*., A review on air cooled and air centric hybrid thermal management techniques for Li-ion battery packs in electric vehicles, *Journal of Energy Storage, 41* (2021), pp. 102885

[5] Wu, W., *et al*., An innovative battery thermal management with thermally induced flexible phase change material, *Energy Conversion and Management, 221* (2020), pp. 113145

[6] Liu, Z., *et al*., Numerical study of thermal management of pouch lithium-ion battery based on composite liquid-cooled phase change materials with honeycomb structure, *Journal of Energy Storage, 70* (2023), pp. 108001

[7] Fan, R., *et al*., Evaluation of fin intensified phase change material systems for thermal management of Li-ion battery modules, *International Journal of Heat and Mass Transfer, 166* (2021), pp. 120753

[8] Ding, Y., *et al*., Parameters of liquid cooling thermal management system effect on the Li-ion battery temperature distribution, *Thermal Science, 26* (2022), 1B, pp. 567-577

[9] Liu, Z., *et al*., Experimental study on the thermal management of batteries based on the coupling of composite phase change materials and liquid cooling, *Applied Thermal Engineering, 185* (2021), pp. 116415

[10] Zhang, J., *et al*., Numerical evaluation of the heat transfer performance of water-cooled system for electric vehicle drive motor based on the field synergy principle, *Thermal Science,* Online First (2023), https://doi.org/10.2298/TSCI230422164Z

[11] Kuang, N., *et al*., The study of heat characteristics for micro pin-fin heat sinks with different structures, *Thermal Science,* Online First (2023), https://doi.org/10.2298/TSCI230311175K

[12] Ren, H., *et al*., Experimental investigation on pouch lithium-ion battery thermal management with mini-channels cooling plate based on heat generation characteristic, *Journal of Thermal Science, 31* (2022), 3, pp. 816-829

[13] Koorata, P. K., *et al.*, Thermal management of large-sized $LiFePO_4$ pouch cell using simplified mini-channel cold plates, *Applied Thermal Engineering, 234* (2023), pp. 121286

[14] Wang, Z., *et al*., Numerical simulation of heat transfer and flow characteristics for plate fin-and-tube heat exchanger with ring-bridge slit fins. *Thermal Science,* Online First (2023), https://doi.org/10.2298/TSCI230123096W

[15] Joshi, A. K., *et al*., Computational analysis of preheating cylindrical lithium-ion batteries with fin-assisted phase change material, *International Journal of Modern Physics C*, (2023), pp. 2450047, https://doi.org/10.1142/S0129183124500475

[16] Talele, V., *et al*., Computational modelling and statistical evaluation of thermal runaway safety regime response on lithium-ion battery with different cathodic chemistry and varying ambient condition, *International Communications in Heat and Mass Transfer, 146* (2023), pp.106907

[17] Yang, R., *et al*., Comparative study on the thermal characteristics of solid-state lithium-ion batteries, *IEEE Transactions on Transportation Electrification*, June 27, 2023, doi: 10.1109/TTE.2023.3289997

[18] Chen, J., *et al*., A convolutional neural network for estimation of lithium-ion battery state-of-health during constant current operation, *Proceedings*, 2023 IEEE Transportation Electrification Conference & Expo (ITEC), IEEE, Chiang Mai, Thailand, 2023, pp.1-6

[19] Subhedar, D., *et al.*, Numerical investigation of performance for liquid-cooled cylindrical electrical vehicle battery pack using Al2O3/EG-water nano coolant, *Materials Today: Proceedings*, Aug. 19, 2023, https://doi.org/10.1016/j.matpr.2023.08.055

[20] Jiang, G., *et al*., Experiment and simulation of thermal management for a tube-shell Li-ion battery pack with composite phase change material, *Applied Thermal Engineering, 120* (2017), pp. 1-9

[21] Liu, H., *et al*., Investigation into the effectiveness of nanofluids on the mini-channel thermal management for high power lithium-ion battery, *Applied Thermal Engineering, 142* (2018), pp. 511-523

[22] Bahiraei, F., *et al*., Electrochemical-thermal modeling to evaluate active thermal management of a lithium-ion battery module, *Electrochimica Acta, 254* (2017), pp. 59-71

[23] Wei, S., Study on thermal environment simulation of high-density lithium battery, MA. Sc thesis, Zhongyuan University of Technology, Zhoengzhou, China, 2016

[24] Liu, Y., *et al*., Design a J-type air-based battery thermal management system through surrogate-based optimization, *Applied Energy*, *252* (2019), pp. 113426

[25] Yousefi, E., *et al*., The effect of different enclosure materials and NePCMs on performance of battery thermal management system, *Materials Today: Proceedings*, *75* (2023), pp. 1-9

[26] Wu, X., *et al*., Structural optimization of light-weight battery module based on hybrid liquid cooling with high latent heat PCM, *International Journal of Heat and Mass Transfer*, *163* (2020) pp. 120495

[27] Wang, Y., *et al.*, Thermal performance predictions for an HFE-7000 direct flow boiling cooled battery thermal management system for electric vehicles, *Energy Conversion and Management*, *207* (2020), pp. 112569

Received: 30.10.2023.
Revised: 18.02.2024.
Accepted: 06.03.2024.